Radboud Repository

Radboud University Nijmegen

PDF hosted at the Radboud Repository of the Radboud University Nijmegen

The following full text is a preprint version which may differ from the publisher's version.

For additional information about this publication click this link.
http://hdl.handle.net/2066/124948

Multi-photon production in e^+e^- collisions at $\sqrt{s} = 183$ GeV

The OPAL Collaboration

Abstract

The process $e^+e^- \rightarrow \gamma\gamma(\gamma)$ is studied using data recorded with the OPAL detector at LEP. The data sample corresponds to a total integrated luminosity of 56.2 pb^{-1} taken at a centre-of-mass energy of 183 GeV. The measured cross-section agrees well with the expectation from QED. A fit to the angular distribution is used to obtain improved limits at 95% CL on the QED cut-off parameters: $\Lambda_+ > 233$ GeV and $\Lambda_- > 265$ GeV as well as a mass limit for an excited electron, $M_{e^*} > 227$ GeV assuming equal $e^*e\gamma$ and $ee\gamma$ couplings. No evidence for resonance production is found in the invariant mass spectrum of photon pairs. Limits are obtained for the cross-section times branching ratio for a resonance decaying into two photons.

(To be submitted to Phys. Lett.)

The OPAL Collaboration

K. Ackerstaff[8], G. Alexander[23], J. Allison[16], N. Altekamp[5], K.J. Anderson[9], S. Anderson[12], S. Arcelli[2], S. Asai[24], S.F. Ashby[1], D. Axen[29], G. Azuelos[18,a], A.H. Ball[17], E. Barberio[8], R.J. Barlow[16], R. Bartoldus[3], J.R. Batley[5], S. Baumann[3], J. Bechtluft[14], T. Behnke[8], K.W. Bell[20], G. Bella[23], S. Bentvelsen[8], S. Bethke[14], S. Betts[15], O. Biebel[14], A. Biguzzi[5], S.D. Bird[16], V. Blobel[27], I.J. Bloodworth[1], M. Bobinski[10], P. Bock[11], J. Böhme[14], M. Boutemeur[34], S. Braibant[8], P. Bright-Thomas[1], R.M. Brown[20], H.J. Burckhart[8], C. Burgard[8], R. Bürgin[10], P. Capiluppi[2], R.K. Carnegie[6], A.A. Carter[13], J.R. Carter[5], C.Y. Chang[17], D.G. Charlton[1,b], D. Chrisman[4], C. Ciocca[2], P.E.L. Clarke[15], E. Clay[15], I. Cohen[23], J.E. Conboy[15], O.C. Cooke[8], C. Couyoumtzelis[13], R.L. Coxe[9], M. Cuffiani[2], S. Dado[22], G.M. Dallavalle[2], R. Davis[30], S. De Jong[12], L.A. del Pozo[4], A. de Roeck[8], K. Desch[8], B. Dienes[33,d], M.S. Dixit[7], M. Doucet[18], J. Dubbert[34], E. Duchovni[26], G. Duckeck[34], I.P. Duerdoth[16], D. Eatough[16], P.G. Estabrooks[6], E. Etzion[23], H.G. Evans[9], F. Fabbri[2], A. Fanfani[2], M. Fanti[2], A.A. Faust[30], F. Fiedler[27], M. Fierro[2], H.M. Fischer[3], I. Fleck[8], R. Folman[26], A. Fürtjes[8], D.I. Futyan[16], P. Gagnon[7], J.W. Gary[4], J. Gascon[18], S.M. Gascon-Shotkin[17], C. Geich-Gimbel[3], T. Geralis[20], G. Giacomelli[2], P. Giacomelli[2], V. Gibson[5], W.R. Gibson[13], D.M. Gingrich[30,a], D. Glenzinski[9], J. Goldberg[22], W. Gorn[4], C. Grandi[2], E. Gross[26], J. Grunhaus[23], M. Gruwé[27], G.G. Hanson[12], M. Hansroul[8], M. Hapke[13], C.K. Hargrove[7], C. Hartmann[3], M. Hauschild[8], C.M. Hawkes[5], R. Hawkings[27], R.J. Hemingway[6], M. Herndon[17], G. Herten[10], R.D. Heuer[8], M.D. Hildreth[8], J.C. Hill[5], S.J. Hillier[1], P.R. Hobson[25], A. Hocker[9], R.J. Homer[1], A.K. Honma[28,a], D. Horváth[32,c], K.R. Hossain[30], R. Howard[29], P. Hüntemeyer[27], P. Igo-Kemenes[11], D.C. Imrie[25], K. Ishii[24], F.R. Jacob[20], A. Jawahery[17], H. Jeremie[18], M. Jimack[1], A. Joly[18], C.R. Jones[5], P. Jovanovic[1], T.R. Junk[8], D. Karlen[6], V. Kartvelishvili[16], K. Kawagoe[24], T. Kawamoto[24], P.I. Kayal[30], R.K. Keeler[28], R.G. Kellogg[17], B.W. Kennedy[20], A. Klier[26], S. Kluth[8], T. Kobayashi[24], M. Kobel[3,e], D.S. Koetke[6], T.P. Kokott[3], M. Kolrep[10], S. Komamiya[24], R.V. Kowalewski[28], T. Kress[11], P. Krieger[6], J. von Krogh[11], P. Kyberd[13], G.D. Lafferty[16], D. Lanske[14], J. Lauber[15], S.R. Lautenschlager[31], I. Lawson[28], J.G. Layter[4], D. Lazic[22], A.M. Lee[31], E. Lefebvre[18], D. Lellouch[26], J. Letts[12], L. Levinson[26], R. Liebisch[11], B. List[8], C. Littlewood[5], A.W. Lloyd[1], S.L. Lloyd[13], F.K. Loebinger[16], G.D. Long[28], M.J. Losty[7], J. Ludwig[10], D. Liu[12], A. Macchiolo[2], A. Macpherson[30], M. Mannelli[8], S. Marcellini[2], C. Markopoulos[13], A.J. Martin[13], J.P. Martin[18], G. Martinez[17], T. Mashimo[24], P. Mättig[26], W.J. McDonald[30], J. McKenna[29], E.A. Mckigney[15], T.J. McMahon[1], R.A. McPherson[28], F. Meijers[8], S. Menke[3], F.S. Merritt[9], H. Mes[7], J. Meyer[27], A. Michelini[2], S. Mihara[24], G. Mikenberg[26], D.J. Miller[15], R. Mir[26], W. Mohr[10], A. Montanari[2], T. Mori[24], K. Nagai[26], I. Nakamura[24], H.A. Neal[12], B. Nellen[3], R. Nisius[8], S.W. O'Neale[1], F.G. Oakham[7], F. Odorici[2], H.O. Ogren[12], M.J. Oreglia[9], S. Orito[24], J. Pálinkás[33,d], G. Pásztor[32], J.R. Pater[16], G.N. Patrick[20], J. Patt[10], R. Perez-Ochoa[8], S. Petzold[27], P. Pfeifenschneider[14], J.E. Pilcher[9], J. Pinfold[30], D.E. Plane[8], P. Poffenberger[28], B. Poli[2], J. Polok[8], M. Przybycień[8], C. Rembser[8], H. Rick[8], S. Robertson[28], S.A. Robins[22], N. Rodning[30], J.M. Roney[28], K. Roscoe[16], A.M. Rossi[2], Y. Rozen[22], K. Runge[10], O. Runolfsson[8], D.R. Rust[12], K. Sachs[10], T. Saeki[24], O. Sahr[34], W.M. Sang[25], E.K.G. Sarkisyan[23], C. Sbarra[29], A.D. Schaile[34], O. Schaile[34], F. Scharf[3], P. Scharff-Hansen[8], J. Schieck[11], B. Schmitt[8], S. Schmitt[11], A. Schöning[8], T. Schorner[34], M. Schröder[8], M. Schumacher[3], C. Schwick[8], W.G. Scott[20], R. Seuster[14], T.G. Shears[8], B.C. Shen[4], C.H. Shepherd-Themistocleous[8], P. Sherwood[15],

G.P. Siroli[2], A. Sittler[27], A. Skuja[17], A.M. Smith[8], G.A. Snow[17], R. Sobie[28],
S. Söldner-Rembold[10], M. Sproston[20], A. Stahl[3], K. Stephens[16], J. Steuerer[27], K. Stoll[10],
D. Strom[19], R. Ströhmer[34], R. Tafirout[18], S.D. Talbot[1], S. Tanaka[24], P. Taras[18], S. Tarem[22],
R. Teuscher[8], M. Thiergen[10], M.A. Thomson[8], E. von Törne[3], E. Torrence[8], S. Towers[6],
I. Trigger[18], Z. Trócsányi[33], E. Tsur[23], A.S. Turcot[9], M.F. Turner-Watson[8], R. Van Kooten[12],
P. Vannerem[10], M. Verzocchi[10], P. Vikas[18], H. Voss[3], F. Wäckerle[10], A. Wagner[27], C.P. Ward[5],
D.R. Ward[5], P.M. Watkins[1], A.T. Watson[1], N.K. Watson[1], P.S. Wells[8], N. Wermes[3],
J.S. White[28], G.W. Wilson[14], J.A. Wilson[1], T.R. Wyatt[16], S. Yamashita[24], G. Yekutieli[26],
V. Zacek[18], D. Zer-Zion[8]

[1]School of Physics and Astronomy, University of Birmingham, Birmingham B15 2TT, UK
[2]Dipartimento di Fisica dell' Università di Bologna and INFN, I-40126 Bologna, Italy
[3]Physikalisches Institut, Universität Bonn, D-53115 Bonn, Germany
[4]Department of Physics, University of California, Riverside CA 92521, USA
[5]Cavendish Laboratory, Cambridge CB3 0HE, UK
[6]Ottawa-Carleton Institute for Physics, Department of Physics, Carleton University, Ottawa, Ontario K1S 5B6, Canada
[7]Centre for Research in Particle Physics, Carleton University, Ottawa, Ontario K1S 5B6, Canada
[8]CERN, European Organisation for Particle Physics, CH-1211 Geneva 23, Switzerland
[9]Enrico Fermi Institute and Department of Physics, University of Chicago, Chicago IL 60637, USA
[10]Fakultät für Physik, Albert Ludwigs Universität, D-79104 Freiburg, Germany
[11]Physikalisches Institut, Universität Heidelberg, D-69120 Heidelberg, Germany
[12]Indiana University, Department of Physics, Swain Hall West 117, Bloomington IN 47405, USA
[13]Queen Mary and Westfield College, University of London, London E1 4NS, UK
[14]Technische Hochschule Aachen, III Physikalisches Institut, Sommerfeldstrasse 26-28, D-52056 Aachen, Germany
[15]University College London, London WC1E 6BT, UK
[16]Department of Physics, Schuster Laboratory, The University, Manchester M13 9PL, UK
[17]Department of Physics, University of Maryland, College Park, MD 20742, USA
[18]Laboratoire de Physique Nucléaire, Université de Montréal, Montréal, Quebec H3C 3J7, Canada
[19]University of Oregon, Department of Physics, Eugene OR 97403, USA
[20]Rutherford Appleton Laboratory, Chilton, Didcot, Oxfordshire OX11 0QX, UK
[22]Department of Physics, Technion-Israel Institute of Technology, Haifa 32000, Israel
[23]Department of Physics and Astronomy, Tel Aviv University, Tel Aviv 69978, Israel
[24]International Centre for Elementary Particle Physics and Department of Physics, University of Tokyo, Tokyo 113, and Kobe University, Kobe 657, Japan
[25]Institute of Physical and Environmental Sciences, Brunel University, Uxbridge, Middlesex UB8 3PH, UK
[26]Particle Physics Department, Weizmann Institute of Science, Rehovot 76100, Israel
[27]Universität Hamburg/DESY, II Institut für Experimental Physik, Notkestrasse 85, D-22607 Hamburg, Germany

[28]University of Victoria, Department of Physics, P O Box 3055, Victoria BC V8W 3P6, Canada
[29]University of British Columbia, Department of Physics, Vancouver BC V6T 1Z1, Canada
[30]University of Alberta, Department of Physics, Edmonton AB T6G 2J1, Canada
[31]Duke University, Dept of Physics, Durham, NC 27708-0305, USA
[32]Research Institute for Particle and Nuclear Physics, H-1525 Budapest, P O Box 49, Hungary
[33]Institute of Nuclear Research, H-4001 Debrecen, P O Box 51, Hungary
[34]Ludwigs-Maximilians-Universität München, Sektion Physik, Am Coulombwall 1, D-85748 Garching, Germany

[a] and at TRIUMF, Vancouver, Canada V6T 2A3
[b] and Royal Society University Research Fellow
[c] and Institute of Nuclear Research, Debrecen, Hungary
[d] and Department of Experimental Physics, Lajos Kossuth University, Debrecen, Hungary
[e] on leave of absence from the University of Freiburg

1 Introduction

This paper reports a study of the process $e^+e^- \rightarrow \gamma\gamma(\gamma)$ using data recorded with the OPAL detector at LEP at an average centre-of-mass energy of 182.7 GeV with an integrated luminosity of 56.2 pb^{-1}. At LEP energies, this is one of the few processes having negligible contributions from the weak interaction. Since the QED differential cross-section is precisely predicted by theory [1, 2], searches for deviations from the expected angular distribution are a sensitive probe for non-standard physics processes contributing to these photonic final states. Any non-QED effects described by the general framework of effective Lagrangian theory are expected to increase with centre-of-mass energy [3]. A comparison of the measured photon angular distribution with the QED expectation can be used to place limits on the QED cut-off parameters $\Lambda_\pm$, contact interactions ($e^+e^-\gamma\gamma$) and non-standard $e^+e^-\gamma$-couplings as described in section 3. The possible existence of an excited electron, e^*, which would also change the angular distribution [4], is investigated. In addition, a search is made for the possible production of a resonance X via $e^+e^- \rightarrow X\gamma$, followed by the decay $X \rightarrow \gamma\gamma$, using the invariant mass spectrum of photon pairs in three-photon final states.

The process $e^+e^- \rightarrow \gamma\gamma(\gamma)$ has been analysed previously at lower energies [5, 6, 7, 8]. The main differences from the previous OPAL analysis at $\sqrt{s} = 130 - 172$ GeV [5] are an increased angular acceptance and an improved rejection of non-physics backgrounds. The following section contains a brief description of the OPAL detector and of the Monte Carlo simulated event samples. Section 3 describes the QED differential cross-sections for $e^+e^- \rightarrow \gamma\gamma(\gamma)$, as well as those from several models describing extensions to QED. In sections 4 – 6 the analysis is described in detail. The results are presented in section 7.

2 The OPAL detector and Monte Carlo samples

A detailed description of the OPAL detector can be found in Ref. [9]. The polar angle, θ, is measured with respect to the electron-beam direction and ϕ is the azimuthal angle. For this analysis the most important detector component is the electromagnetic calorimeter (ECAL) which is divided into two parts, the barrel and the endcaps. The barrel covers polar angles with $|\cos\theta| < 0.82$ and consists of 9440 lead-glass blocks in a quasi-pointing geometry. The endcaps cover the polar angle range $0.81 < |\cos\theta| < 0.98$ and each consists of 1132 blocks. The spatial resolution is about 11 mm, corresponding to $0.2°$ in θ. The energy resolution for high energy photons is about 1.6% in the barrel and $3 - 5\%$ in the endcaps depending on the angle. The ECAL surrounds the tracking chambers. Hit information from the jet chamber and the vertex drift chamber is used to reject events which are consistent with having charged particles coming from the interaction point. Outside the ECAL are the hadronic calorimeter (HCAL), which is incorporated into the magnet yoke, and beyond that the muon chambers. Both the HCAL and the muon chambers are used to reject cosmic ray events.

Various Monte Carlo samples are used to study the selection efficiency and expected background contributions. For the signal process $e^+e^- \rightarrow \gamma\gamma(\gamma)$ the RADCOR [2] generator is used, while FGAM [10] is used for $e^+e^- \rightarrow \gamma\gamma\gamma\gamma$. FGAM does not take into account the electron mass and hence can not be used if at least one photon is along the beam-axis. The Bhabha process

is simulated using BHWIDE [11] and TEEGG [12]. The processes $e^+e^- \to \overline{\nu}\nu\gamma(\gamma)$, $\mu^+\mu^-$ and $\tau^+\tau^-$ are simulated using KORALZ [13]. PYTHIA [14] is used for hadronic events. All samples were processed through the OPAL detector simulation program [15] and reconstructed in the same way as real data.

3 Cross-section for the process $e^+e^- \to \gamma\gamma$

The Born-level differential cross-section for the process $e^+e^- \to \gamma\gamma$, in the relativistic limit of lowest order QED is given by [16]:

$$\left(\frac{d\sigma}{d\Omega}\right)_{\text{Born}} = \frac{\alpha^2}{s} \frac{1 + \cos^2\theta}{1 - \cos^2\theta} \,, \tag{1}$$

where s denotes the square of the centre-of-mass energy, α is the fine-structure constant and the event angle θ is the polar angle of one photon. Since the two photons cannot be distinguished, the event angle is defined such that $\cos\theta$ is positive.

In Ref. [1] possible deviations from the QED cross-section for Bhabha and Møller scattering are parametrized in terms of cut-off parameters $\Lambda_\pm$. These parameters correspond to a short-range exponential term added to the Coulomb potential. This ansatz leads to a modification of the photon angular distribution of the form

$$\left(\frac{d\sigma}{d\Omega}\right)_{\Lambda_\pm} = \left(\frac{d\sigma}{d\Omega}\right)_{\text{Born}} \left[1 \pm \frac{s^2}{2\Lambda_\pm^4} \sin^2\theta\right]. \tag{2}$$

Alternatively, in terms of effective Lagrangian theory, a gauge-invariant operator may be added to QED. Depending on the dimension of the operator, different deviations from QED can be formulated [3]. Contact interactions ($\gamma\gamma e^+e^-$) or non-standard γe^+e^- couplings described by dimension 6, 7 or 8 operators lead to angular distributions with different mass scales Λ. In most cases these deviations are functionally similar [5]. The cross-section predicted by a dimension-7 Lagrangian is given by

$$\left(\frac{d\sigma}{d\Omega}\right)_{\Lambda'} = \left(\frac{d\sigma}{d\Omega}\right)_{\text{Born}} + \frac{s^2}{32\pi} \frac{1}{\Lambda'^6} \,. \tag{3}$$

The existence of an excited electron e^* with an $e^*e\gamma$ coupling would contribute to the photon production process via t-channel exchange. The resulting deviation from $\left(\frac{d\sigma}{d\Omega}\right)_{\text{Born}}$ depends on the e^* mass M_{e^*} and the coupling constant κ of the $e^*e\gamma$ vertex relative to the $ee\gamma$ vertex [4]:

$$\left(\frac{d\sigma}{d\Omega}\right)_{e^*} = \left(\frac{d\sigma}{d\Omega}\right)_{\text{Born}} + f(M_{e^*}, \kappa, s, \cos\theta). \tag{4}$$

The function f is explicitly given in Ref. [5]. In the limit $M_{e^*} \gg \sqrt{s}$, $\left(\frac{d\sigma}{d\Omega}\right)_{e^*}$ approaches $\left(\frac{d\sigma}{d\Omega}\right)_{\Lambda_\pm}$ with the mass related to the cut-off parameter by $M_{e^*} = \sqrt{\kappa}\,\Lambda_+$.

In a multi-photon event, it is important to choose an appropriate definition of the event angle. The event angle is not uniquely defined since the two highest energy photons in general are not exactly back-to-back. The event angle $\cos\theta^*$ used in this paper is defined as

$$\cos\theta^* = \left| \sin\frac{\theta_1 - \theta_2}{2} \right| \bigg/ \left(\sin\frac{\theta_1 + \theta_2}{2} \right) , \tag{5}$$

where θ_1 and θ_2 are the polar angles of the two highest energy photons. This definition was chosen such that the deviations in the angular distribution with respect to the Born level are small, in this case between $3 - 6\%$ for $\cos\theta^* < 0.996$ as was shown in Ref. [5]. For two-photon final states $\cos\theta^*$ is identical to $|\cos\theta|$ and for three-photon events in which the third photon is along the beam direction, θ^* is equivalent to the scattering angle in the centre-of-mass system of the two observed photons. Since the angular definition is based on the two highest energy photons of the event, events with one of those escaping detection along the beam-axis are rejected from the analysis.

4   Event selection

Events are selected by requiring two or more clusters of energy in the electromagnetic calorimeter (ECAL). A cluster is selected as a photon candidate if it is within the polar angle range $|\cos\theta| < 0.97$. The cluster must consist of at least two lead-glass blocks and the cluster energy has to exceed 1 GeV (uncorrected for possible energy loss in the material before the ECAL).

There are two major classes of background. The first class consists of events without primary charged tracks. Certain cosmic ray events, beam halo and the Standard Model process $e^+e^- \to \bar{\nu}\nu\gamma\gamma$ contribute to this background. The second class can be identified by the presence of primary charged tracks. Bhabha events, for example, have similar electromagnetic cluster characteristics to $\gamma\gamma(\gamma)$ events, but are distinguished by the presence of tracks in the central tracking chambers.

Rejection of non-physics backgrounds

A cosmic-ray particle can pass through the hadronic and electromagnetic calorimeters without producing a reconstructed track in the central tracking chambers. These particles do not cross the beam-axis. Since the HCAL and ECAL have different radii, the resulting hits in the two detectors occur separated in azimuth. To remove this background, we reject events with 3 or more track segments found in the muon chambers. In the case of fewer than three such track segments, the event rejection depends on the highest energy HCAL cluster of the event. Events are rejected if this HCAL cluster is separated from each of the photon candidates by more than $10°$ in azimuth and has at least 1 GeV of deposited energy in the case of one or two muon track segments or 15% of the observed ECAL energy if no muon track segments are found.

Another type of background consists of events with large occupancy in the ECAL well localised in the detector. To reject these events, cuts on the extent of adjoining clusters are applied. An event is rejected if one of these accumulations consists of more than 12 ECAL clusters or has

an extent of more than 0.4 rad in θ or 0.4 rad/$\sin\theta$ in ϕ. After these cuts, the remaining non-physics background has low visible energy and becomes negligible after the kinematic selection described below.

Kinematic requirements

The selection is based primarily on the requirement of small missing energy and small missing transverse momentum. Selection variables based on the measured angles and assuming three-body kinematics are used where possible. In the case of four or more photons no constraints are available.

The event sample is divided into four classes *I– IV* which are distinguished by the number of photon candidates N_γ, the acollinearity angle $\xi_{\rm acol}$ and the aplanarity angle $\xi_{\rm aplan}$:

$$\xi_{\rm acol} = 180° - \alpha_{12} \tag{6}$$
$$\xi_{\rm aplan} = 360° - (\alpha_{12} + \alpha_{13} + \alpha_{23}), \tag{7}$$

where α_{ij} is the angle between clusters i and j and the two highest energy clusters are labelled 1, 2.

All events having an acollinearity angle $\xi_{\rm acol} < 10°$ (i.e., with the two highest energy clusters almost collinear) are assigned to class I, independent of the number of photon candidates. For true $e^+e^- \to \gamma\gamma(\gamma)$ events in this class, the sum of the two highest cluster energies $E_S^I = E_1 + E_2$ should be close to the centre-of-mass energy $\sqrt{s}$. Events in class I are selected if $E_S^I > 0.6\sqrt{s}$.

Class II consists of acollinear events ($\xi_{\rm acol} > 10°$) with exactly two observed photon candidates. Events of this class typically contain an energetic photon that escapes detection near the beam-axis ($|\cos\theta| > 0.97$). If the polar angle of this photon is approximated as $|\cos\theta| = 1$, its energy, $E_{\rm lost}$, can be estimated from the angles of the observed clusters θ_1 and θ_2:

$$E_{\rm lost} = \sqrt{s}\left(1 + \frac{\sin\theta_1 + \sin\theta_2}{|\sin(\theta_1 + \theta_2)|}\right)^{-1}. \tag{8}$$

The energy sum E_S^{II} is calculated by summing the two observed cluster energies and the lost energy:

$$E_S^{II} = E_1 + E_2 + E_{\rm lost}. \tag{9}$$

The imbalance $\mathcal{B}$, defined as

$$\mathcal{B} = (\sin\theta_1 + \sin\theta_2)\left|\cos\left(\frac{\phi_1 - \phi_2}{2}\right)\right|, \tag{10}$$

provides an approximate measure of the scaled transverse momentum of the event. Events in class II are selected if $\mathcal{B} < 0.2$, $E_S^{II} > 0.6\sqrt{s}$ and $E_{\rm lost}$ is less than both E_1 and E_2. This last requirement ensures that the two highest energy photons are those observed.

Classes III and IV contain acollinear events ($\xi_{\rm acol} > 10°$) having 3 or more observed photon candidates. In this case the cluster energies must be used in addition to the cluster angles in

calculating the transverse and longitudinal momenta (p_t, p_l) of the system. Since a non-zero longitudinal momentum could result from an additional unobserved photon along the beam direction, the energy sum E_S^{III} is calculated by adding p_l to the cluster energies E_i:

$$E_S^{III} = \sum_{i=1}^{N_\gamma} E_i + p_l \, . \tag{11}$$

Events in classes III and IV are selected if $E_S^{III} > 0.6\sqrt{s}$ and $p_t < 0.1\sqrt{s}$. Again, the lost energy along the beam-axis, now determined by p_l, must be smaller than the energies of the two highest energy clusters.

Figure 1 shows the aplanarity distribution for selected events in classes III and IV for data and for the $\mathcal{O}(\alpha^3)$ Monte Carlo after the charged-event rejection described in the next section. Most events are planar ($\xi_{\mathrm{aplan}} < 0.1°$) and are well described by the Monte Carlo. They are consistent with exactly three produced photons as simulated by the Monte Carlo. There are, however, 5 aplanar events ($\xi_{\mathrm{aplan}} > 0.1°$). These events can be explained by the production of a fourth photon that escapes detection along the beam-axis in most cases. Planar events with exactly 3 observed photon candidates are assigned to class III and aplanar three-photon events and events with more than three observed photon candidates are assigned to class IV.

The signal events are well separated from non-physics background in terms of energy and transverse momentum as has been demonstrated at lower energies [5]. The non-physics background is reduced to a negligible level after the above described kinematic requirements which are summarised in Table 1.

Event class	I	II	III	IV
Number of photon candidates	$N_\gamma \geq 2$	$N_\gamma = 2$	$N_\gamma = 3$	$N_\gamma \geq 3$
Acollinearity	$\xi_{\mathrm{acol}} < 10°$	$\xi_{\mathrm{acol}} > 10°$	$\xi_{\mathrm{acol}} > 10°$	$\xi_{\mathrm{acol}} > 10°$
Aplanarity			$\xi_{\mathrm{aplan}} < 0.1°$	$\xi_{\mathrm{aplan}} > 0.1°$
Energy sum	$E_S^I > 0.6\sqrt{s}$	$E_S^{II} > 0.6\sqrt{s}$	$E_S^{III} > 0.6\sqrt{s}$	$E_S^{III} > 0.6\sqrt{s}$
Transverse momentum		$\mathcal{B} < 0.2$	$p_t < 0.1\sqrt{s}$	$p_t < 0.1\sqrt{s}$
Longitudinal momentum		$E_{\mathrm{lost}} < E_1, E_2$	$p_l < E_1, E_2$	$p_l < E_1, E_2$

Table 1: Summary of the kinematic cuts. For definition of the variables see the text. In the case of more than three observed photons in class IV there is no requirement on the aplanarity.

Charged-event rejection

The rejection of all events having tracks in the central tracking chambers would lead to an efficiency loss because of photon conversions. Nevertheless, contributions from any channel with primary charged tracks must be reduced to a negligible level. To achieve this, events are rejected if they have a large number of hits in the inner part of the drift chambers as described in Ref. [5]. In addition, events are rejected if there is a reconstructed track separated by more than 10° in azimuth from all photon candidates. A good agreement of the efficiency and

charged track rejection power has been observed between data and Monte Carlo for different combinations of the vetoes.

5 Corrections and systematic errors

Since the deviations from QED (Equations 2 – 4) are given with respect to Born level, the observed angular distribution is corrected to Born level. The effect of radiative corrections is quantified by $\mathcal{R}$, the ratio of the angular distribution of the $e^+e^- \to \gamma\gamma(\gamma)$ Monte Carlo and the Born-level cross-section:

$$\mathcal{R} = \left(\frac{d\sigma}{d\Omega}\right)_{\mathrm{MC}} (\cos\theta^*) \bigg/ \left(\frac{d\sigma}{d\Omega}\right)_{\mathrm{Born}}. \tag{12}$$

The ratio $\mathcal{R}$ varies between 1.03 and 1.06 within the studied angular range and is used to correct the data bin by bin to Born level. A 1% systematic error from higher-order effects is taken to be correlated between all bins.

The efficiency and angular resolution of the reconstruction are determined using an $\mathcal{O}(\alpha^3)$ Monte Carlo sample with full detector simulation. In the angular range $\cos\theta^* < 0.87$ the efficiency varies smoothly between $90 - 94\%$ and a polynomial parametrisation is used for the correction. For the rest of the angular range the efficiency drops rapidly and a bin-by-bin (bin width = 0.01) correction is made. The main reason for the loss is photon conversion. As a conservative estimate, the systematic error on the efficiency is taken to be a quarter of the inefficiency. The resulting error ranges from 1.5% ($\cos\theta^* < 0.55$) to 15% ($\cos\theta^* > 0.96$). The 1.5% error is taken to be correlated between all bins.

The agreement between generated and reconstructed event angles is very good; an event-angle resolution of $0.2°$ is obtained. In addition, the cluster angle has been compared to the track angle for Bhabha events. For clusters with $|\cos\theta| > 0.96$ the cluster angle is systematically about $0.4°$ closer to the beam-axis than the track angle. For all other clusters the difference is less than $0.1°$. Due to the cut-off at $\cos\theta^* < 0.97$ this would lead to a decrease of the measured total cross-section by 1.1% if this effect is caused by the cluster angle. It is included in the systematic error on the total cross-section.

The luminosity is derived from small-angle Bhabha scattering measured on both sides of the detector in the polar angle region 34 mrad $< \theta <$ 56 mrad. Uncertainties in the selection and in the theoretical cross-section, as well as a 30 MeV uncertainty on the beam energy lead to a systematic error of 0.5% which is taken into account.

Table 2 shows the number of selected events from the data and from the expected Standard Model sources after the different selection cuts. The preselected data have a large contribution from non-physics backgrounds until the kinematic cuts are applied. There is little efficiency loss up to this point. The restriction on the missing longitudinal momentum (E_{lost} for class *II*) rejects events with a high-energy photon escaping along the beam-axis. About 97% of the remaining sample consists of Bhabha events and is well described by the Monte Carlo. After the charged-event rejection about one background event is expected which is negligible compared to the expected $\gamma\gamma(\gamma)$ signal.

9

Cut	Data	MC	$\gamma\gamma(\gamma)$	$e^+e^-(\gamma)$	$e\gamma(e)$	$\tau^+\tau^-$	$\mu^+\mu^-$	$\nu\bar{\nu}\gamma\gamma$	$q\bar{q}$
Preselection	92833	37822	780	27778	3010	325	32	18	5879
Non-physics bg. reject.	55791	32029	777	27657	2977	127	1.7	18	471
Kinematic req.	28456	29263	769	26673	1760	32	0.6	1.1	27
$E_{\text{lost}}, p_l < E_1, E_2$	25284	26504	714	25707	62	8.7	<0.1	<0.1	12
Charged event reject.	620	603	602	0.3	0.6	<0.1	<0.1	<0.1	<0.1

Table 2: Number of selected events after the different cuts described in the text. The numbers are given for the data and the sum of Monte Carlo samples with the breakdown by final states given in the following columns. The BHWIDE generator is labelled by $e^+e^-(\gamma)$ and TEEGG by $e\gamma(e)$. All Monte Carlo predictions are normalised to the integrated luminosity of the data.

6 Results

Cross-section

In Table 3 the numbers of observed events in the different kinematic classes are compared to the Monte Carlo expectation. Since there is no Monte Carlo generator for the case of a four-photon event where at least one photon is along the beam axis, no prediction for class *IV* events with three observed photons is given. The prediction for events with four or more observed photons is calculated using FGAM. One event with four detected photons is observed. The total cross-section σ for the process $e^+e^- \rightarrow \gamma\gamma(\gamma)$ determined from 620 events selected in the range $\cos\theta^* < 0.97$ is also given in Table 3. The total error is statistics dominated. The cross-section is corrected for detection efficiency and $\mathcal{O}(\alpha^3)$ effects derived from $\mathcal{R}$ (Eq. 12). The cross-section at the different LEP energies as measured by OPAL in the range $\cos\theta^* < 0.9$ is shown in Figure 2. All measurements are in good agreement with the QED prediction.

The angular distribution of the observed events and the measured differential cross-section, obtained by applying efficiency and radiative corrections, are shown in Figure 3. The data have a $\chi^2/\text{NDF} = 12.1/20$ with respect to the QED expectation (solid line). The 95% CL interval of a χ^2-fit to the data of the function $\left(\frac{d\sigma}{d\Omega}\right)_{\Lambda_\pm}$ (Eq. 2) is also shown (dashed line). To obtain the

Class	*I*	*II*	*III*	*IV*		all	cross-section [pb]	
N_γ	≥ 2	2	3	3	≥ 4	events	$\cos\theta^* < 0.9$	$\cos\theta^* < 0.97$
observed	558	46	11	4	1	620	8.4 ± 0.4	12.9 ± 0.7
expected	546	44.6	11.3	–	0.42	602	8.0	12.5

Table 3: Number of observed and expected events in the angular range $\cos\theta^* < 0.97$ for different classes. N_γ is the number of observed photon candidates. The total cross-section is corrected to Born level and is given for two angular ranges to allow comparison of these results with those of previous OPAL measurements. The errors are dominated by statistics.

limits at 95% confidence level the probability is normalised to the physically allowed region, i.e. $\Lambda_+ > 0$ and $\Lambda_- < 0$ as described in Ref. [17]. For both functions $\left(\frac{d\sigma}{d\Omega}\right)_{\Lambda_\pm}$ and $\left(\frac{d\sigma}{d\Omega}\right)_{\Lambda'}$ the χ^2 distribution is parabolic as a function of the chosen fitting parameters $\Lambda_\pm^{-4}$ and Λ'^{-6}. The asymmetric limits $\lambda_\pm$ on the fitting parameter can be obtained by:

$$\frac{\int_0^{\lambda_+} G(x,\mu,\sigma)dx}{\int_0^\infty G(x,\mu,\sigma)dx} = 0.95 \qquad \text{and} \qquad \frac{\int_{\lambda_-}^0 G(x,\mu,\sigma)dx}{\int_{-\infty}^0 G(x,\mu,\sigma)dx} = 0.95 \; , \qquad (13)$$

where G is a Gaussian with the central value and error of the fit result denoted by μ and σ, respectively.

The limit on the mass of an excited electron M_{e^*} as a function of the coupling constant κ for the $(e^*e\gamma)$-vertex, which is fixed during the fit, is shown in Figure 4. In the case of $\left(\frac{d\sigma}{d\Omega}\right)_{e^*}$ the cross-section does not depend linearly on the chosen fitting parameter $M_{e^*}^{-2}$ and the limit corresponds to an increase of the χ^2 by 3.84 with respect to the minimum.

The fit results are summarised in Table 4. All results are from the data taken at 183 GeV. The inclusion of the data taken at $130 - 172$ GeV does not substantially improve the results. The limits obtained are roughly 40 GeV higher than our previous results. Similar limits are obtained by ALEPH and DELPHI at 183 GeV [18].

Fit parameter	Fit result	95% CL Limit [GeV]
$\Lambda_\pm^{-4}$	$(1.04 \pm 1.34) \cdot 10^{-10}$ GeV^{-4}	$\Lambda_+ > 233$
		$\Lambda_- > 265$
Λ'^{-6}	$(1.11 \pm 1.29) \cdot 10^{-17}$ GeV^{-6}	$\Lambda' > 557$
$M_{e^*}^{-2}$	$\left(1.06 {}^{+0.51}_{-3.23}\right) \cdot 10^{-5}$ GeV^{-2}	$M_{e^*} > 227$

Table 4: Fit results and 95% CL lower limits obtained from the fit to the differential cross-section. The limit for the mass of an excited electron is determined assuming the coupling constant $\kappa = 1$.

Resonance production

A resonance X produced by the process $e^+e^- \to X\gamma$ and decaying into two photons, $X \to \gamma\gamma$, could be seen in the two-photon invariant mass spectrum, since this process leads to a three-photon final state without missing energy. Searches for such a resonance have been performed previously at the Z^0 peak [19] and at higher energies [5, 6], leading to bounds on Higgs and gauge boson interactions [20]. For this search, 16 events from classes *III* and *IV* are used. The invariant mass of each photon pair is shown separately for class *III* (Figure 5a) and class *IV* (Figure 5b).

For class *III* the energies of the three photons are not based on the measured cluster energies but are calculated from the photon angles assuming three body kinematics:

$$E_k \propto \sin\alpha_{ij} \; ; \; E_1 + E_2 + E_3 = \sqrt{s}, \qquad (14)$$

with E_k the energy of one photon and α_{ij} the angle between the other two photons. In this case a typical mass resolution for photon pairs is about 0.5 GeV. For class-IV events the invariant mass is calculated from the measured cluster energies and angles with a typical mass resolution of 3 GeV.

The distribution obtained from class-III events is consistent with the Monte Carlo expectation from the QED process $e^+e^- \to \gamma\gamma(\gamma)$ as seen in Figure 5a. In neither the class-III nor the class-IV distribution is there evidence for an enhancement due to a resonance. An upper limit on the total production cross-section multiplied by the photonic branching ratio is calculated using the method of Ref. [21]. This method uses fractional event counting where the weights assigned to each photon pair depend on the expected resolution and the difference between the hypothetical and the reconstructed mass. The limits shown in Figure 6 are obtained using only class-III events assuming the natural width of the resonance to be negligible. The $e^+e^- \to \gamma\gamma(\gamma)$ background is subtracted. For the efficiency correction the production and subsequent decay of the resonance are assumed to be isotropic. The mass range is limited by the acollinearity restriction. Regarding a model with anomalous couplings of the Higgs boson [20] this analysis gives access to a larger mass range than the analysis of $e^+e^- \to HZ$ with $H \to \gamma\gamma$.

7   Conclusions

The process $e^+e^- \to \gamma\gamma(\gamma)$ has been studied using data taken with the OPAL detector at a centre-of-mass energy of 183 GeV. The measured angular distribution and total cross-section for this process both agree well with QED predictions. The limits (95% CL) on cut-off parameters are $\Lambda_+ > 233$ GeV, $\Lambda_- > 265$ GeV and $\Lambda' > 557$ GeV. An excited electron is excluded for $M_{e^*} > 227$ GeV assuming the $e^*e\gamma$ and $ee\gamma$ coupling to be the same. In the $\gamma\gamma$ invariant mass spectrum using events with at least three final-state photons, no evidence is found for a resonance X decaying to $\gamma\gamma$. A limit on the production cross-section times branching ratio is derived as a function of the mass M_X. One event with four detected photons is observed.

8   Acknowledgements

References

[1] S.D. Drell, Ann. Phys. **4** (1958) 75.

[2] F.A. Berends and R. Kleiss, Nucl. Phys. **B186** (1981) 22.

[3] O.J.P. Éboli, A.A. Natale and S.F. Novaes, Phys. Lett. **B271** (1991) 274.

[4] A. Litke, Ph.D.Thesis, Harvard University, unpublished (1970).

[5] OPAL Collaboration, K. Ackerstaff et al., Eur. Phys. J. **C1** (1998) 21.

[6] L3 Collaboration, M. Acciarri et al., Phys. Lett. **B413** (1997) 159.

[7] ALEPH Collaboration, D. Buskulic et al., Phys. Lett. **B384** (1996) 333.

[8] DELPHI Collaboration, P. Abreu et al., Phys. Lett. **B268** (1991) 296.

[9] OPAL Collaboration, K. Ahmet et al., Nucl. Instr. and Meth. **A305** (1991) 275.

[10] CALCUL Collaboration, F.A. Berends et al., Nucl. Phys. **B239** (1984) 395;
P. Janot, PhD Thesis, LAL 87-31 (1987).

[11] S. Jadach et al., Phys. Lett. **B390** (1997) 298.

[12] D. Karlen, Nucl. Phys. **B289** (1987) 23.

[13] S. Jadach et al., Comp. Phys. Comm. **66** (1991) 276.

[14] T. Sjöstrand and M. Bengtsson, Comp. Phys. Comm. **43** (1987) 367;
T. Sjöstrand, Comp. Phys. Comm. **39** (1986) 347.

[15] OPAL Collaboration, J. Allison et al., Nucl. Instr. and Meth. **A317** (1992) 47.

[16] I. Harris and L.M. Brown, Phys. Rev. **105** (1957) 1656;
F.A. Berends and R. Gastmans, Nucl. Phys. **B61** (1973) 414.

[17] Review of Particle Physics, R.M. Barnett et al., Phys. Rev. **D54** (1996) 164.

[18] ALEPH Collaboration, R. Barate et al., CERN-EP/98-053, submitted to Phys. Lett. B;
DELPHI Collaboration, P. Abreu et al., CERN-EP/98-075, submitted to Phys. Lett. B.

[19] OPAL Collaboration, P.D. Acton et al., Phys. Lett. **B311** (1993) 391;
L3 Collaboration, M. Acciarri et al., Phys. Lett. **B345** (1995) 609.

[20] O.J.P. Éboli, M.C. Gonzalez-Garcia, S.M. Lietti and S.F. Novaes, hep-ph/9802408 (1998).

[21] P. Bock, Heidelberg preprint HD-PY 96/05, submitted to Nucl. Instrum. Meth. .

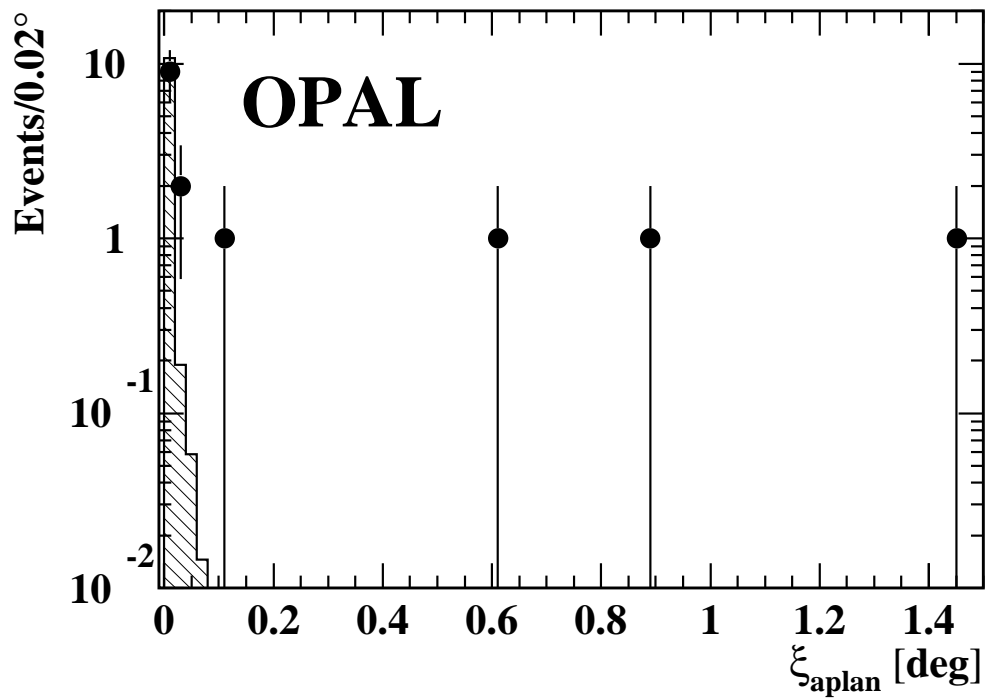[22] OPAL Collaboration, M.Z. Akrawy et al., Phys. Lett **B257** (1991) 531.

Figure 1: The aplanarity for selected events with three or more photons (classes *III* and *IV*). The points show the data and the histogram represents the $\mathcal{O}(\alpha^3)$ Monte Carlo expectation normalised to the integrated luminosity of the data. One additional event is observed at $\xi_{\mathrm{aplan}} = 4.8°$.
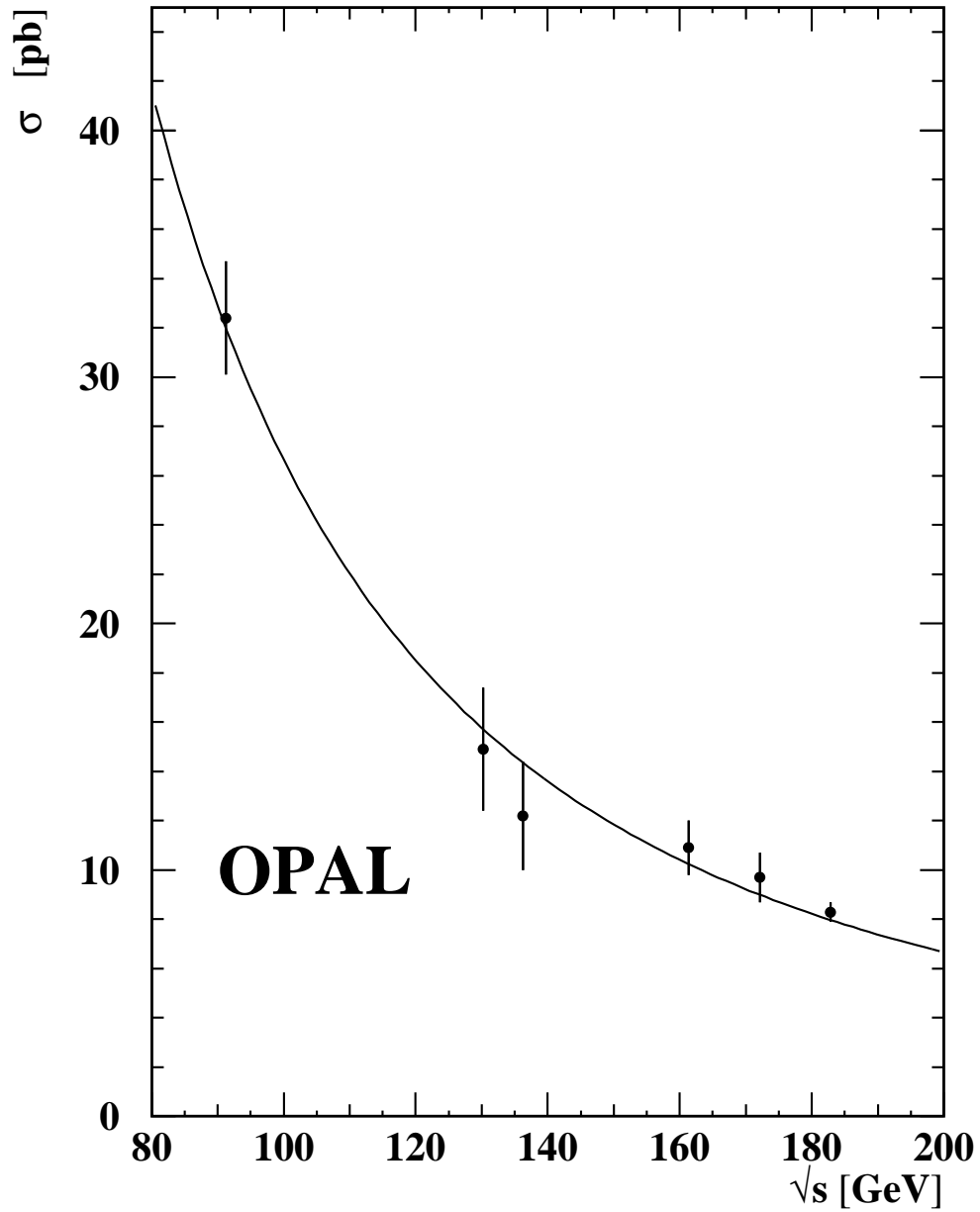
Figure 2: Total cross-section for the process $e^+e^- \rightarrow \gamma\gamma$ with $\cos\theta^* < 0.9$. The data are corrected for efficiency loss and higher-order effects and correspond to Born level. Results at lower energies are taken from [5, 22]. The curve shows the Born-level QED expectation.
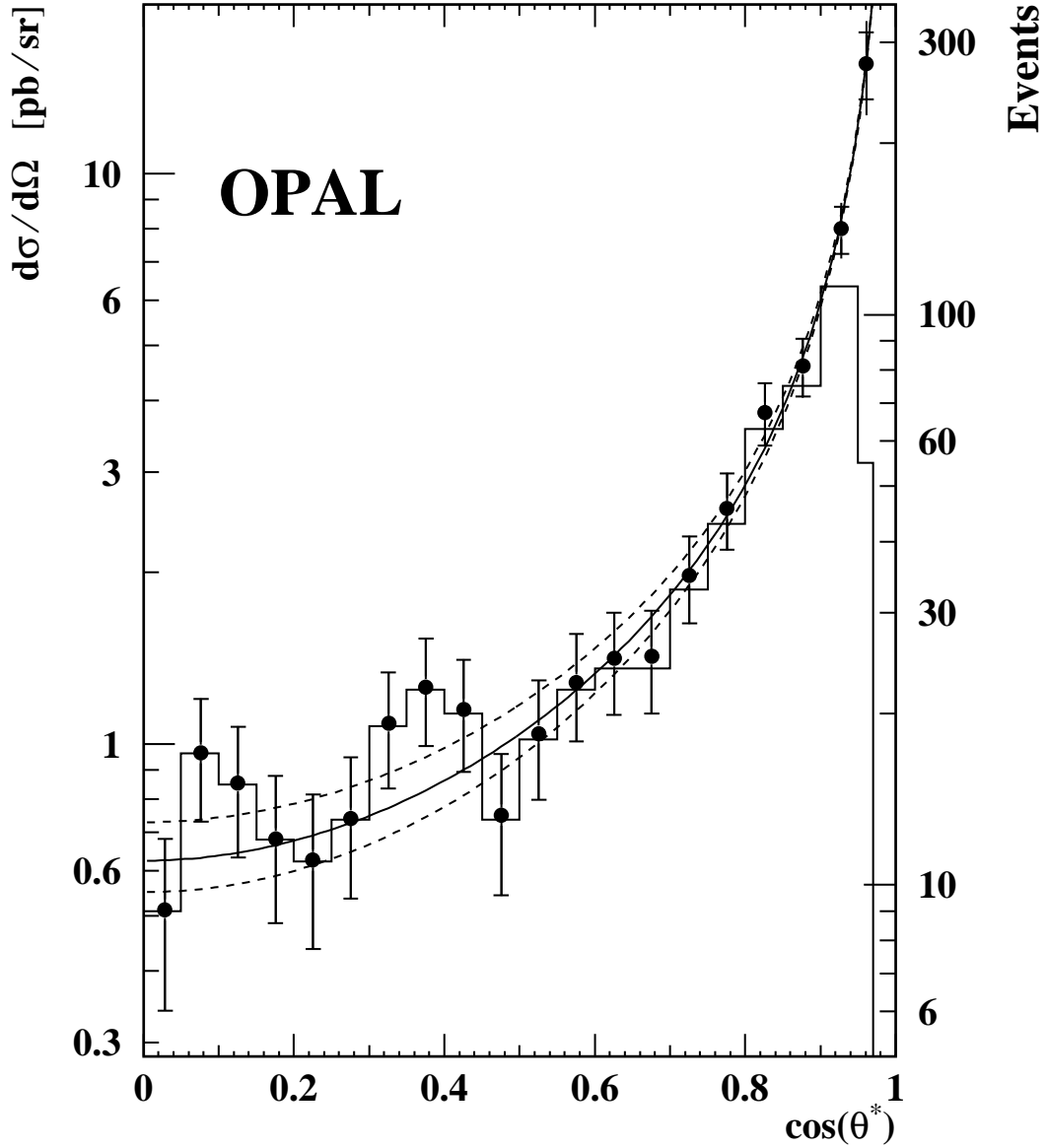
Figure 3: The measured angular distribution for the process $e^+e^- \rightarrow \gamma\gamma(\gamma)$ at $\sqrt{s} = 183$ GeV. The histogram shows the observed number of events per bin. Note the smaller width of the highest $\cos\theta^*$ bin. The points show the number of events corrected for efficiency and radiative effects. The inner error-bars correspond to the statistical error and the outer error-bars to the total error. The solid curve corresponds to the Born-level QED prediction. The dashed lines represent the 95% CL interval of the fit to the function $\left(\frac{d\sigma}{d\Omega}\right)_{\Lambda_\pm}$.
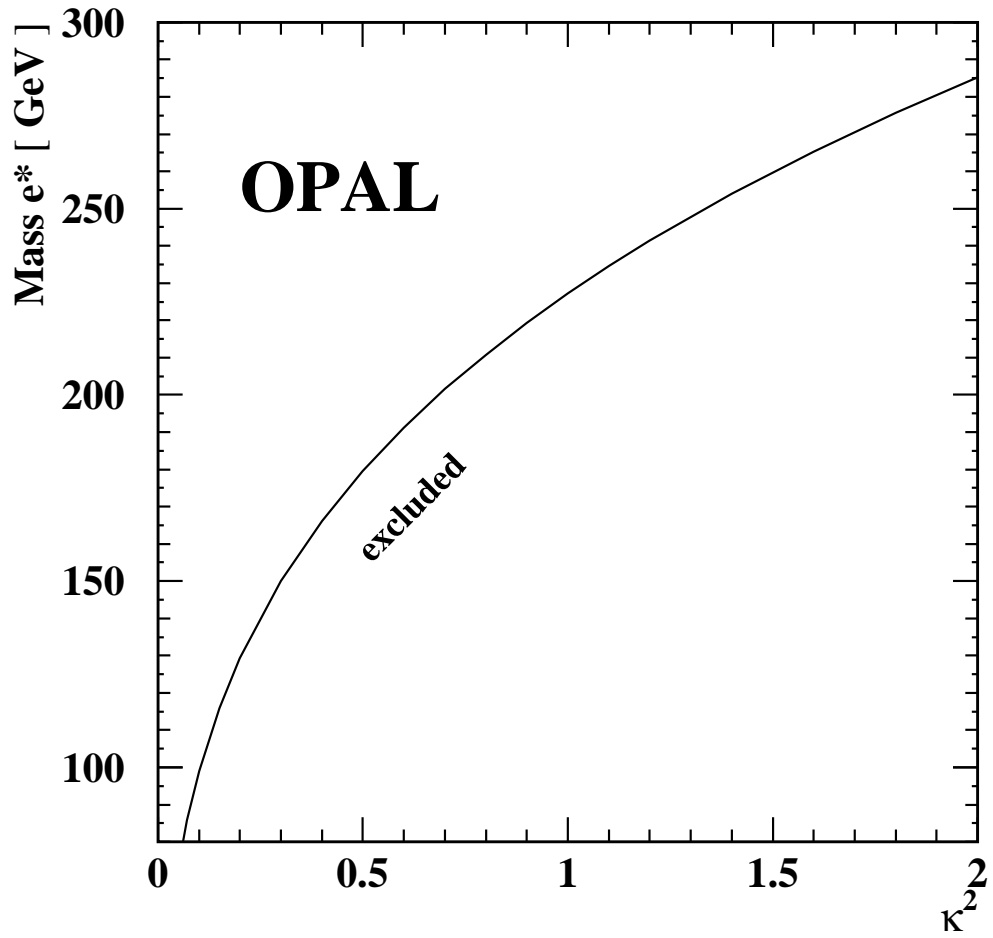
Figure 4: Lower limit (95% CL) on the mass M_{e^*} of an excited electron as a function of the square of the $e^*e\gamma$ coupling constant κ^2.
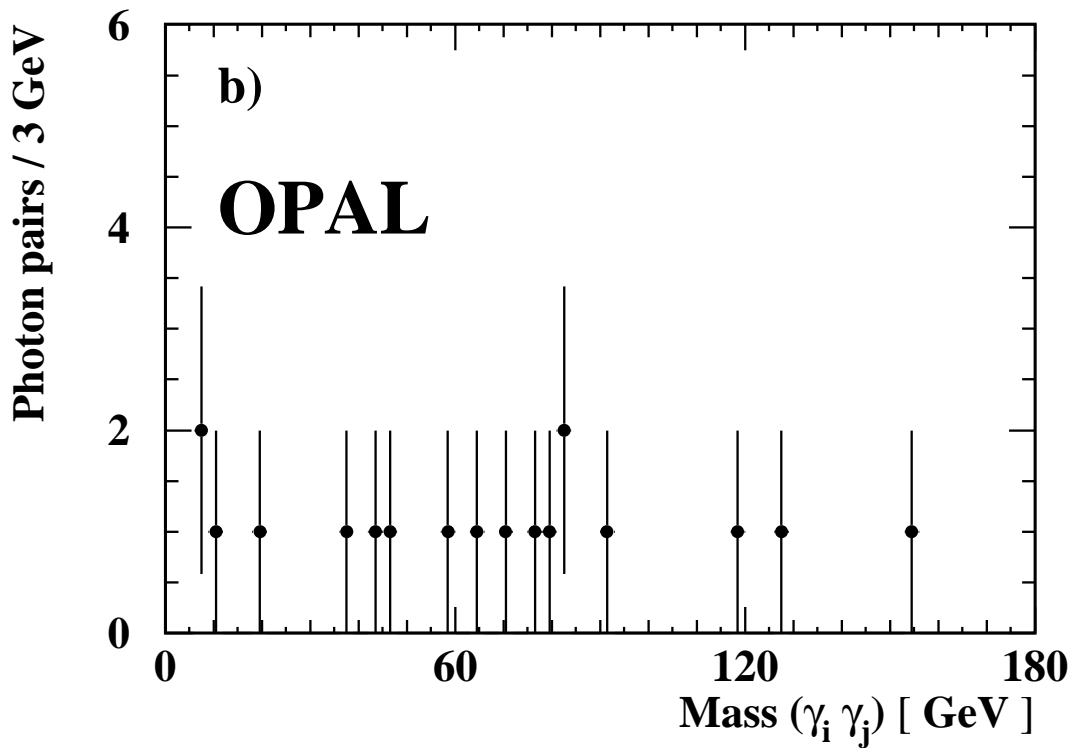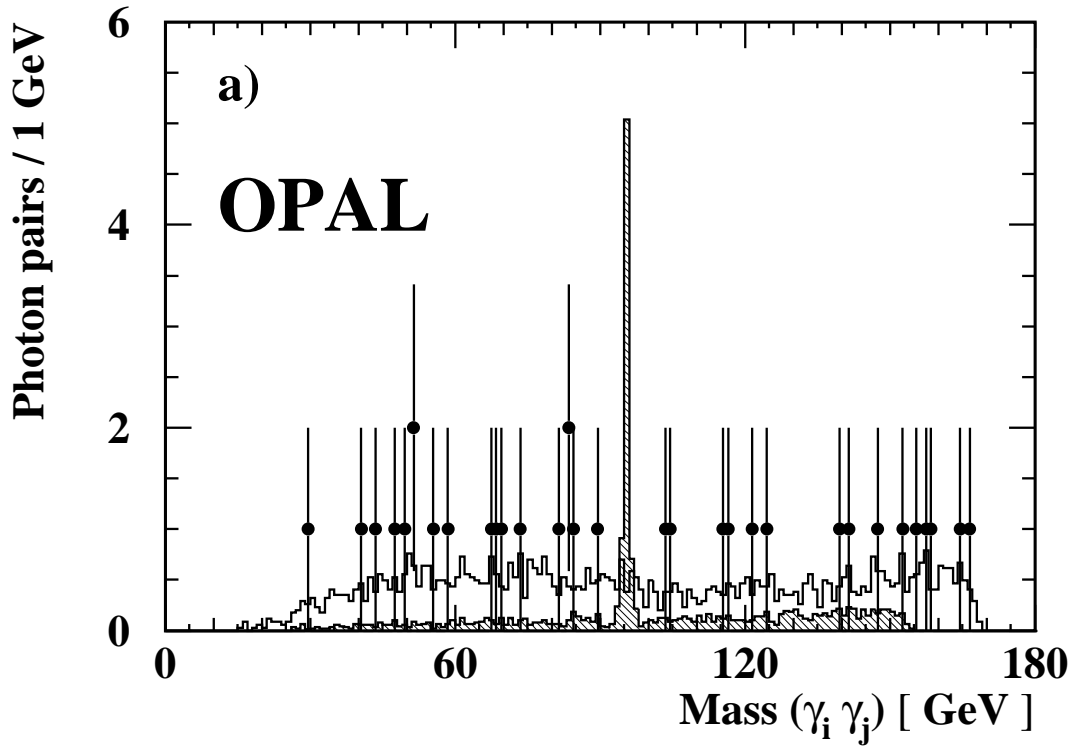
Figure 5: The invariant mass of photon pairs from a) class-*III* and b) class-*IV* events. The points are the data and the open histogram the $e^+e^- \to \gamma\gamma(\gamma)$ Monte Carlo expectation scaled by a factor of two for clarity. The hatched histogram in a) represents a $\gamma\gamma$ resonance at 95.5 GeV with a cross-section times branching ratio of 0.10 pb. In each case, the binning is chosen to match the expected mass resolution.
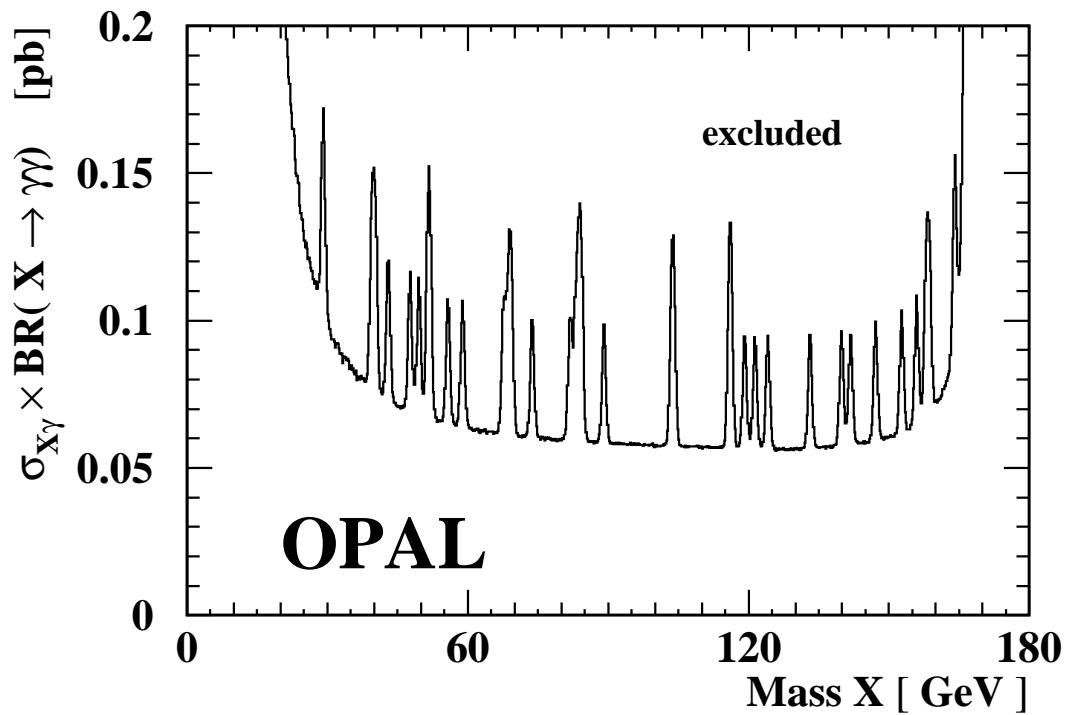
18

Figure 6: Upper limit (95% CL) for the cross-section times branching ratio for the process $e^+e^- \rightarrow X\gamma$, $X \rightarrow \gamma\gamma$ as a function of the mass of the resonance X. Only class-*III* events are used for this result.